JOURNAL OF GUIDANCE, CONTROL, AND DYNAMICS
Vol. 29, No. 2, March–April 2006

Adaptive Model Inversion Control of a Helicopter with Structural Load Limiting

Nilesh A. Sahani* and Joseph F. Horn†
Pennsylvania State University, University Park, Pennsylvania 16802

An adaptive control system capable of providing consistent handling qualities throughout the operational flight envelope is a desirable feature for rotorcraft. The adaptive model inversion controller with structural load limit protection evaluated here offers the capability to adapt to changing flight conditions along with aggressive maneuvering without envelope limit violations. The controller was evaluated using a nonlinear simulation model of the UH-60 helicopter. The controller is based on a well-documented model inversion architecture with an adaptive neural network (ANN) to compensate for inversion error. The ANN was shown to improve the tracking ability of the controller at off-design point flight conditions; although at some flight conditions the controller performed well even without adaptation. The controller was modified to include a structural load-limiting algorithm to avoid exceeding prescribed limits on the longitudinal hub moment. The limiting was achieved by relating the hub moment to pitch acceleration. The acceleration limits were converted to pitch angle command limits imposed in the pitch axis command filter. Results show that the longitudinal hub moment response in aggressive maneuvers stayed within the prescribed limits for a range of operating conditions. The system was effective in avoiding the longitudinal hub moment limit without unnecessary restrictions on the aircraft performance.

Nomenclature

A, B	=	state-space inversion model matrices
a	=	aircraft acceleration, ft/s^2
$\boldsymbol{e}$	=	error vector
h_r	=	distance between main rotor hub and aircraft c.g., ft
I_{xx}, I_{yy}, I_{zz}, I_{xz}	=	aircraft moments of inertia at body axes, slug $\cdot$ ft^2
K	=	feedback gain
K_P, K_I, K_D	=	constants for proportional–integral–derivatives error dynamics
K_β, K_{hub}	=	individual blade and total hub spring constant
M	=	aircraft total pitching moment at c.g., ft $\cdot$ lb
M_a	=	aircraft mass, slug
M_f	=	fuselage aerodynamic pitching moment at c.g., ft $\cdot$ lb
M_H	=	longitudinal hub moment, ft $\cdot$ lb
N_b	=	number of rotor blades
p, q, r	=	roll, pitch, and yaw rates, rad/s
S_{HT}	=	area of horizontal tail, ft^2
s, c	=	short notation for sine and cosine
T	=	main rotor thrust, lb
$\boldsymbol{U}$	=	pseudocontrol vector
U_{ad}	=	adaptive neural network output
u, v, w	=	body velocities, ft/s
V	=	total velocity, ft/s
W	=	neural network weight vector/aircraft weight, lb
x, y, z	=	aircraft body axes
Z_{HT}	=	lift at horizontal tail, lb
β	=	basis vector for adaptive neural network
β_{1s}, β_{1c}	=	lateral and longitudinal flapping angles, rad
δ_{lat}, δ_{lon}, δ_{ped}	=	lateral, longitudinal, and pedal control input, in.
ϕ, θ, ψ	=	roll, pitch, and yaw angles, deg
ω, ζ	=	frequency and damping ratio of command filter dynamics, rad/s, nondimensional

Subscripts

c	=	command filter output
cmd	=	pilot command
D	=	desired accelerations
HT	=	horizontal tail
lim	=	limiting value
u, l	=	corresponding to upper and lower limit, respectively
ϕ, θ, ψ	=	quantities corresponding to roll, pitch, and yaw channel, respectively
0	=	values at trim condition

Superscript

$\sim$	=	error between actual and commanded inputs

I. Introduction

TO meet the ADS-33 handling qualities requirements and to meet more stringent agility requirements of future rotorcraft missions, flight control designers for military rotorcraft must tackle a number of challenging problems.[1] Demanding military mission requirements will require high-bandwidth flight controllers capable of performing aggressive maneuvers. Like their counterparts in the fixed wing industry, rotorcraft flight control designers often deal with inherently unstable airframes that can exhibit a good deal of nonlinearity in maneuvering flight. In addition, rotorcraft tend to exhibit significant cross-coupling effects and tend to be more restricted by structural constraints than their fixed-wing counterparts. As a result, it is a major challenge to achieve consistently desirable handling characteristics over the entire flight envelope. The design methods used on modern military rotorcraft such as the RAH-66 and V-22 have been shown to be effective.[2] However, the cost and time associated with refining the flight control laws is becoming substantial, and there is still much room for improvement in achieving desirable handling qualities in the extreme portions of the envelope.

The two main challenges for achieving consistent handling qualities over the entire flight envelope are 1) that the aircraft flight dynamics can change significantly for different operating points and

Received 27 October 2004; revision received 7 February 2005; accepted for publication 8 February 2005. Copyright © 2005 by the American Institute of Aeronautics and Astronautics, Inc. All rights reserved. Copies of this paper may be made for personal or internal use, on condition that the copier pay the $10.00 per-copy fee to the Copyright Clearance Center, Inc., 222 Rosewood Drive, Danvers, MA 01923; include the code 0731-5090/06 $10.00 in correspondence with the CCC.

*Graduate Research Assistant, Department of Aerospace Engineering. Student Member AIAA.

†Assistant Professor, Department of Aerospace Engineering. Senior Member AIAA.

aircraft configurations and 2) that the aircraft must fly at extreme portions of the flight envelope without exceeding limits. On rotorcraft, these limits are often defined in terms of structural or controllability constraints. Monitoring and avoiding these limits can result in significant pilot workload.[3,4] The addition of high-bandwidth flight control laws on rotorcraft will aggravate this problem because a high-bandwidth response requires higher angular accelerations and, therefore, results in larger control moments in maneuvering flights. These moments will lead to increased loads on the rotor mast as well as other components.

The inherent nonlinearity of all aircraft results in different linearized dynamics at different operating points. On supersonic aircraft the dynamics can change drastically as the aircraft transitions from low-speed flight to supersonic flight. On rotorcraft, flight dynamics vary substantially between the low-speed/hover mode and forward flight. In addition, various mission requirements may require that the aircraft operate in different configurations, for example, different sets of external stores. The configuration changes result in significant changes in the mass properties and aerodynamic characteristics of the aircraft.

Dynamic model inversion is a popular feedback linearization method for achieving consistent response characteristics.[5] It tracks the commanded accelerations or angular rates by computing the required control time history using a known plant model. The technique has been applied in flight for providing control augmentation in high-performance aircraft[6] and has been found to be effective for high angle of attack fighter aircraft.[7] A drawback of this technique is its sensitivity to modeling error.[8] The method requires accurate representations of the aircraft dynamics throughout the operational flight envelope. Developing an exhaustive schedule of dynamic models then becomes a major driver in the cost and time associated with the flight control design. Obtaining these data from flight test is expensive, and safety concerns make it difficult to obtain models very close to envelope limits. Simulation models can be used, but accuracy is a major concern, especially for rotorcraft simulation models that have known deficiencies. For this purpose, an adaptive neural network-based approach was proposed in Refs. 9 and 10. In this approach, a single linear model was used for model inversion control, and an adaptive neural network was used to compensate the error between the linear model and the actual response. The technique was used to provide consistent handling qualities for a tilt-rotor simulation model,[11] and has been tested in flight for a helicopter unmanned aerial vehicle (UAV).[12] In the present work, the technique is used to provide consistent handling qualities on a full-scale helicopter and is demonstrated using a high-fidelity blade element simulation model.

The capability to alleviate pilot workload associated with monitoring and avoiding envelope limits has been a priority for the rotorcraft handling qualities community over the last 15 years. This capability is sometimes referred to as carefree maneuvering. A number of new techniques that allow the pilot to fly very close to the envelope limit have been developed.[3,4,13–19] These techniques include implementation of special cueing systems as well as enhancements to the flight control laws. New approaches have been proposed to predict the onset of limit and to calculate the constraints on the control input.[13–15] The constraints can then be relayed to the pilot through tactile cues on the pilot's control inceptor or by imposing constraints in the flight control system. A limit avoidance function that acts through the automatic flight control system in the context of an adaptive model inversion controller is investigated in this paper. One advantage of the model inversion architecture is that it achieves direct tracking of the aircraft fast states and the first derivatives of these states. If a structural limit can be directly related to the fast states and their first derivatives, then structural load limiting can be achieved by imposing internal limits in the command filter. Furthermore, an adaptive controller would be expected to track the commands very accurately, and, thus, there should be reasonable certainty that the structural limits would be observed. The strategy of constraining the command inputs has been used for limit avoidance in a helicopter UAV.[16] This method implemented an adaptive neural network to represent the relationship between command input and the limit. In the present work, a more straightforward method of relating structural limits to aircraft body rates using dynamic equations is presented, as opposed to using a complex neural network as proposed in Ref. 16. The advantage of the load limiting method proposed in this paper lies in its computational simplicity.

The structural load-limiting algorithm is applied for longitudinal hub moment limit avoidance on a UH-60A helicopter. The main rotor hub moment limit, also known as a mast bending limit, is particularly critical for hingeless rotors that can transfer very high moments to the hub. For example, the RAH-66 encountered hub moment limits during aggressive maneuvers.[2] Limits on the maximum main rotor hub moment can be approached during highly aggressive maneuvers, when the c.g. is near operational limits or during ground operations when the attitude of the aircraft is constrained. In flight, hub moment is a highly dynamic parameter, and limits tend to be reached during the peak response immediately after a large control input or a control reversal. Hub moment limit is most likely to be exceeded in the longitudinal axis because of the higher moment of inertia and larger cyclic control range in the longitudinal axis. A number of different approaches have been developed in the past to compute the limits on control stick corresponding to the hub moment limit.[2,17–19] In this paper, a simplified algorithm that is readily applied to a model inversion type of controller is presented.

The UH-60 simulation model (U.S. Army GENHEL) was selected to demonstrate the controller because it is a high-fidelity simulation model capable of modeling the aircraft performance up to the operational envelope limits. Hub moment limits are not a specific problem on the UH-60 helicopters, and, in fact, the hub moment limit constraints in this study are set artificially low to evaluate the system more rigorously. The objective of this paper is to develop a general approach for including structural load protection in model inversion controllers. Most rotorcraft are designed to sustain worst-case structural loads that would rarely be encountered in operational flight. As a result, most rotorcraft have a significant amount of added structural weight to meet excessive safety margins. Implementing envelope protection systems in future designs or on upgrades of existing rotorcraft would allow the design loads to be relaxed and provide structural weight savings.

This paper is organized as follows. In Sec. II, the adaptive model inversion controller design of Ref. 11 is reviewed and then applied to meet ADS-33D handling qualities specifications for a helicopter. In Sec. III, a method for limiting the longitudinal hub moment is presented. The structural limit is related to aircraft states using basic dynamic equations, and the limits are converted to command input limits in the command filter. In Sec. IV the results generated using a high-fidelity nonlinear simulation model of a helicopter[20] are presented.

II. Adaptive Model Inversion Controller

A. Desired Response

A schematic of the model inversion controller with hub moment limit avoidance is shown in Fig. 1. To obtain the ADS-33D handling qualities specification requirements, an attitude command attitude hold (ACAH) response type was selected for pitch and roll axes and a rate command attitude hold (RCAH) response type was selected for yaw axis. Heave axis was assumed to be uncoupled and independent of the roll, pitch, and yaw axes. Roll and pitch angles were specified as command inputs. A second-order command filter was used to compute the appropriate angular rates and angular accelerations:

$$\ddot{\phi}_c + 2\zeta_\phi \omega_\phi \dot{\phi}_c + \omega_\phi^2 (\phi_c - \phi_{\text{cmd}}) = 0$$

$$\ddot{\theta}_c + 2\zeta_\theta \omega_\theta \dot{\theta}_c + \omega_\theta^2 (\theta_c - \theta_{\text{cmd}}) = 0 \tag{1}$$

For the roll axis, a natural frequency of 3 rad/s and damping ratio of 0.7 was selected. For pitch axis, a natural frequency of 2 rad/s and damping ratio of 0.7 was chosen. In both cases, these values were selected to exceed the ADS-33 level 1 bandwidth requirements for combat rotorcraft.

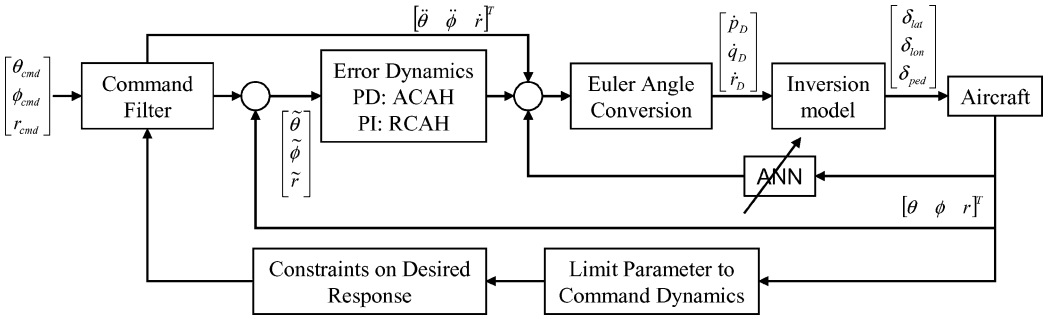

Fig. 1 Schematic of model inversion controller with hub moment limit avoidance.

For yaw axis, yaw rate was specified as the command input. A first-order command filter was selected for this axis. A time constant of 0.25 s was selected to meet the ADS-33 level 1 bandwidth requirements in yaw,

$$\tau_r \dot{r}_c + (r_c - r_{\text{cmd}}) = 0 \tag{2}$$

B. Model Inversion Controller

A model inversion based controller was used to track the command inputs. A 28th-order linear model of the open-loop dynamics for a UH-60A Black Hawk was obtained from the GENHEL simulation model.[20] This higher-order model was reduced to a simple third-order model of angular rate dynamics with lateral, longitudinal, and pedal inputs as control variables,

$$\begin{bmatrix} \dot{p} \\ \dot{q} \\ \dot{r} \end{bmatrix} = [A] \begin{bmatrix} p \\ q \\ r \end{bmatrix} + [B] \begin{bmatrix} \delta_{\text{lat}} \\ \delta_{\text{lon}} \\ \delta_{\text{ped}} \end{bmatrix} \tag{3}$$

The desired acceleration vector (pseudocontrol) was defined using the command filter, feedback control laws, and adaptive neural network output as

$$\boldsymbol{U} = [\dot{p}_D \quad \dot{q}_D \quad \dot{r}_D]^T \tag{4}$$

From this vector, the desired control inputs can be obtained through the model inversion technique as

$$\begin{bmatrix} \delta_{\text{lat}} \\ \delta_{\text{lon}} \\ \delta_{\text{ped}} \end{bmatrix} = [B]^{-1} \left\{ \begin{bmatrix} \dot{p}_D \\ \dot{q}_D \\ \dot{r}_D \end{bmatrix} - [A] \begin{bmatrix} p \\ q \\ r \end{bmatrix} \right\} \tag{5}$$

Tracking error is the difference between the commanded input and the measured response,

$$\tilde{\phi} = \phi_c - \phi, \qquad \tilde{\theta} = \theta_c - \theta, \qquad \tilde{r} = r_c - r \tag{6}$$

The tracking error was minimized by using a proportional–derivative (PD) compensator for the ACAH response in roll and pitch and a proportional–integral (PI) compensator for the RCAH response in yaw. The desired acceleration vector can then be computed as

$$\begin{bmatrix} \ddot{\phi}_D \\ \ddot{\theta}_D \\ \dot{r}_D \end{bmatrix} = \begin{bmatrix} \ddot{\phi}_c \\ \ddot{\theta}_c \\ \dot{r}_c \end{bmatrix} + \begin{bmatrix} K_{P\phi}\tilde{\phi} + K_{D\phi}\dot{\tilde{\phi}} \\ K_{P\theta}\tilde{\theta} + K_{D\theta}\dot{\tilde{\theta}} \\ K_{Pr}\tilde{r} + \int K_{Ir}\tilde{r}\,\mathrm{d}t \end{bmatrix} - \begin{bmatrix} U_{ad\phi} \\ U_{ad\theta} \\ 0 \end{bmatrix} \tag{7}$$

where $U_{ad\phi}$ and $U_{ad\theta}$ are the adaptive neural network contributions that will be discussed in the following section. The PD and PI compensator gains were chosen to specify the error dynamics.[9–11] For the present work, the natural frequency and damping ratio of the error dynamics were set to 3 rad/s and 0.7 for roll and 2.8 rad/s and 0.7 for pitch, respectively. The yaw axis error dynamics were selected to achieve a natural frequency of 4 rad/s and damping ratio of 0.7. Past studies suggested that gains should be selected so that the error dynamics are much faster than the command filter dynamics.[11] However, this resulted in very large feedback gains that generated large control inputs reaching the control authority limits. Selecting large gains also resulted in sustained rotor–body coupling oscillations: the so-called air resonance phenomenon. It was found that selecting the error dynamics to be on the same order as the command filter dynamics produces more reasonable results.

The desired acceleration vector in Eq. (7) is specified using Euler angles whereas the inversion model in Eq. (5) requires angular rates. The following equations can be used for obtaining the desired acceleration vector:

$$\begin{aligned} \dot{p}_D &= \ddot{\phi}_D - (\ddot{\theta}_D s\phi\, s\theta + \dot{r}_D\, s\theta + \dot{\psi}\,\dot{\theta}\, c\phi + \dot{\theta}\,\dot{\phi}\, c\phi\, s\theta \\ &\quad + \dot{\psi}\,\dot{\phi}\, s\theta\, s\phi\, c\theta)/(c\phi\, c\theta) \\ \dot{q}_D &= (\ddot{\theta}_D + \dot{r}_D s\phi + \dot{\psi}\,\dot{\phi}\, c\theta)/c\phi \end{aligned} \tag{8}$$

C. Adaptation Law

When flight conditions change, the actual response of the aircraft can vary significantly from the linear model used for inversion. An adaptive neural network (ANN) approach suggested in Ref. 11 was used here to compensate for the variation. The ANN update law was derived from Lyapunov stability analysis. See Ref. 10 for a detailed derivation; only the update law is presented here.

The ANN approach uses a single-layer sigma–pi neural network. State variables, pseudocontrols, and bias terms are used as input variables. The update law is presented here for the roll axis, and similar equations can be derived for the pitch axis. The output of the sigma–pi neural network, used in Eq. (7), can be written as

$$U_{\text{ad}\phi} = \boldsymbol{W}_\phi^T \boldsymbol{\beta} \tag{9}$$

where $\boldsymbol{W}_\phi^T$ is a neural network weight vector and $\boldsymbol{\beta}$ is a vector of basis functions used as inputs to the neural network. The inputs to the neural network have been categorized into three categories. The basis vector can be derived from these input vectors by means of a Kronecker product,

$$\beta = \text{Kron}[\text{Kron}(C_1, C_2), C_3]$$

$$\text{where} \quad \text{Kron}(x, y) = [x_1 y_1 \quad x_1 y_2 \quad \ldots \quad x_m y_m]^T \tag{10}$$

The first category covers the variation due to airspeed. This category captures the variation of stability and control derivatives with airspeed,

$$C_1 : \{0.1 \quad V \quad V^2\} \tag{11}$$

The second category consists of the state variables and pseudocontrols. It includes body velocities, angular rates, and rotor flapping angles as state variables. This category accounts for nonlinear effects in states, higher-order dynamics associated with rotor flapping, and gain adjustments,

$$C_2 : \{0.1 \;\; u \;\; v \;\; w \;\; p \;\; q \;\; r \;\; \phi \;\; \theta \;\; \beta_{1c} \;\; \beta_{1s} \;\; U_{(1)} \;\; U_{(2)} \;\; U_{(3)}\} \tag{12}$$

The third category is used to include nonlinear effects associated with large roll and pitch angles,

$$C_3 : \{0.1 \quad \phi \quad \theta\} \tag{13}$$

The combination of second and third category effectively introduces square terms on roll and pitch angle to cover nonlinearity at large angles.

The neural network weights are updated at each time step with the update law,

$$\dot{W}_\phi = -\gamma_\phi \boldsymbol{e}_\phi^T P_\phi \boldsymbol{b}\, \beta - \mu_\phi \left\| \boldsymbol{e}_\phi^T P_\phi \boldsymbol{b} \right\| W_\phi \tag{14}$$

Here, $\gamma_\phi > 0$ is the learning rate of the neural network and $\mu_\phi > 0$ is known as the e-modification term. Selection of a higher learning rate increases the speed at which the network adapts, but high learning rates, can make the neural network more sensitive to unmodeled dynamics. For very high learning rates, instabilities were observed. The e-modification term improves robustness to unmodeled dynamics by adding damping and avoiding a pure integral effect in the weight update law. Typically, simulation testing is used to find the proper choice of both the learning rate and e-modification term. The error vector for the roll axis, $\boldsymbol{e}_\phi^T$, is given by

$$\boldsymbol{e}_\phi = [\tilde{\phi} \quad \dot{\tilde{\phi}}]^T \tag{15}$$

The vector $\boldsymbol{b} = [0 \;\; 1]^T$ and P_ϕ is obtained from the Lyapunov stability analysis. It is given by

$$P_\phi = \begin{bmatrix} \dfrac{K_{D\phi}}{K_{P\phi}} + \dfrac{1}{2K_{D\phi}} & \dfrac{1}{2K_{P\phi}} \\ \dfrac{1}{2K_{P\phi}} & \dfrac{1 + K_{P\phi}}{2K_{P\phi}K_{D\phi}} \end{bmatrix} \tag{16}$$

D. Turn Coordination

The lateral control input commands roll attitude of the aircraft. In hover and at low speeds (below 30 kn), the change in roll attitude translates into changes in lateral velocities. In this mode of operation the pilot can control the heading independently using the yaw axis input. However, at higher speeds, the lateral stick input is expected to cause the aircraft to enter a coordinated turn, in which the aircraft heading changes at a rate according to the magnitude of the roll angle and the true airspeed. For this flight condition, the yaw axis feedback controller is used to regulate the lateral acceleration (which is zero in a coordinated turn) instead of the heading. The yaw axis control input can then be used for a lateral acceleration command if the pilot wishes to perform an uncoordinated turn with sideslip. This mode can be realized without changing the inversion controller. An outer loop feedback control is added to calculate the yaw rate command to regulate the lateral acceleration as follows:

$$r_{\text{cmd}} = [K(a_{y\,\text{cmd}} - a_y) + w\, p + g \sin\phi \cos\theta]/u \tag{17}$$

Lateral acceleration command for the yaw axis control input was implemented for velocities above 60 kn, whereas the yaw rate command was preserved for velocities below 30 kn. Between 30 and 60 kn, a smooth transition between the two modes was achieved by linear interpolation of the two commands.

III. Longitudinal Hub Moment Limit Avoidance

An advantage of the proposed architecture is the direct tracking of aircraft states and their derivatives. This offers a novel way of structural load limit avoidance through internal limits in the command filter. In the present work, it is used to avoid exceeding the static hub moment limit. For a dominant part of the flight envelope, the longitudinal hub moment is significantly higher than the lateral component due to the higher inertia and the larger cyclic control range in the longitudinal axis. Therefore, for practical purposes, it is sufficient to restrict the longitudinal hub moment. Because the longitudinal hub moment is related to the pitch acceleration through

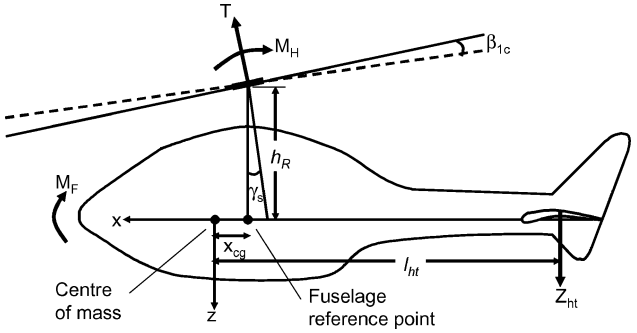

Fig. 2 Pitching moments at aircraft center of mass.

dynamic equations, the longitudinal hub moment limit can be transformed to a limit on the pitch acceleration. This limit can be further converted to a constraint on the pitch angle command that can be implemented in the command filter.

The pitch axis equation of motion is given in Eq. (18). Because of the high moment of inertia in the pitch axis, the effect of off-axis inertia terms can be ignored,

$$M = I_{yy}\dot{q} - (I_{zz} - I_{xx})\, pr - I_{xz}(r^2 - p^2) \approx I_{yy}\dot{q} \tag{18}$$

A simplified form of the pitching moment generated due to rotor forces and aerodynamic surfaces is given in Ref. 21. The forces and moments on a helicopter in the longitudinal plane are shown in Fig. 2. The longitudinal hub moment generated due to the longitudinal flapping (β_{1c}) is a primary contributor to the pitching moment. Note that the hub moment considered in this work is the static longitudinal hub moment, that is, one per revolution component of the longitudinal hub moment. It is not intended to include higher harmonics associated with the vibratory loads. The main rotor thrust T and lift at horizontal tail Z_{HT} also contribute a variable component depending on the c.g. position. The aerodynamic forces at fuselage M_f also contribute to the pitching moment,

$$M = -[(N_b/2)K_\beta + h_R T]\beta_{1c} - (x_{\text{c.g.}} + h_R\gamma_S)T + l_{\text{HT}}(Z_{\text{HT}} + Z_{\text{HT},q}q) + M_f \tag{19}$$

At nonzero forward speed, change in pitch rate changes the angle of attack at the horizontal tail. This changes the lift at the horizontal tail. The change in lift at the horizontal tail due to a unit change in the pitch rate $Z_{\text{HT},q}$ can be written as

$$Z_{\text{HT},q} = -\frac{1}{2}\rho\, V^2 S_{\text{HT}} \left(\frac{\partial C_L}{\partial \alpha}\right)_{\text{HT}} \frac{l_{\text{HT}}}{u} \tag{20}$$

The static longitudinal hub moment can be represented using the longitudinal flapping angle and the hub spring constant as

$$M_H = -(N_b/2)K_\beta\beta_{1c} = -K_{\text{hub}}\beta_{1c} \tag{21}$$

A simplified equation for the thrust in the longitudinal plane can be represented by

$$T \approx -M_a(\ddot{z} - g\cos\theta\, \cos\phi) = -(W/g)a_z \tag{22}$$

Here, $\ddot{z}$ is the z-directional body acceleration. The variable a_z corresponds to the normal load factor and can be measured using inertial sensors. From Eqs. (19–22), the pitching moment can be represented as

$$M \approx (1 + K_1 a_z)\, M_H + K_2 a_z + K_3 q + l_{\text{HT}} Z_{\text{HT}} + M_f$$

$$K_1 = \frac{-h_R W}{g K_{\text{hub}}}, \qquad K_2 = (x_{\text{c.g.}} + h_R\gamma_S)\frac{W}{g}$$

$$K_3 = -\frac{1}{2}\rho\, V^2 S_{\text{HT}} \left(\frac{\partial C_L}{\partial \alpha}\right)_{\text{HT}} \frac{l_{\text{HT}}^2}{u} \tag{23}$$

Aircraft states can be categorized into slow states and fast states according to their response time to a disturbance or control input. Slow states require a larger response time to reach the steady state, for example, body velocities. On the other hand, fast states reach the steady state relatively quickly, for example, angular rates. Dynamic trim is a flight condition where fast states have reached the equilibrium and slow states are varying with time. In this flight condition, the net pitching moment acting on the aircraft is zero. The longitudinal hub moment at the fuselage and the lift at the horizontal tail have very small contributions to the total hub moment in dynamic trim and can be considered to be constant. Therefore, the pitching moment equation (23) in the dynamic trim is

$$0 = (1 + K_1 a_{z0})\, M_{H0} + K_2 a_{z0} + l_{\mathrm{HT}}\, Z_{\mathrm{HT}} + M_f \qquad (24)$$

Here, the subscript zero represents the values in dynamic trim. By the use of this equation, the pitching moment for any flight condition [Eq. (23)] can be rewritten as

$$I_{yy}\dot{q} = (1 + K_1 a_z) M_H - (1 + K_1 a_{z0}) M_{H0} + K_2 (a_z - a_{z0}) + K_3 q \qquad (25)$$

In the implementation, the dynamic trim values were approximated using a first-order lag filter with a time constant of 0.5 s. Using an offline trained neural network is another possible solution to represent these values.

Equation (25) relates the pitch acceleration to the longitudinal hub moment. When the upper and lower limits on longitudinal hub moment are used, the limits on pitch acceleration can be computed as

$$\begin{aligned}\dot{q}_{u\,\mathrm{lim}} &= [(1 + K_1 a_z) M_{Hu\,\mathrm{lim}} - (1 + K_1 a_{z0}) M_{H0} \\ &\quad + K_2 (a_z - a_{z0}) + K_3 q]/I_{yy} \\ \dot{q}_{l\,\mathrm{lim}} &= [(1 + K_1 a_z) M_{Hl\,\mathrm{lim}} - (1 + K_1 a_{z0}) M_{H0} \\ &\quad + K_2 (a_z - a_{z0}) + K_3 q]/I_{yy}\end{aligned} \qquad (26)$$

The pitch acceleration is related to the Euler angle derivatives by Eq. (8). By the rearrangement of the equation, the limits on pitch acceleration can be related to the pitch second derivative of the pitch Euler angle,

$$\ddot{\theta}_{\mathrm{lim}} = \dot{q}_{\mathrm{lim}} c\phi \; - \dot{r}_D\, s\phi - \dot{\psi}\, \dot{\phi}\; c\theta \qquad (27)$$

The model inversion controller described in the preceding section tracks the acceleration commands generated by the command filter. Therefore, the pitch acceleration can be limited by limiting the second derivative of the pitch attitude command in the command filter. The limits on the second derivative can be converted to limits on the pitch angle command by inverting the command filter dynamics,

$$\begin{aligned}\theta_{u\,\mathrm{lim}} &= \theta + (2\zeta_\theta/\omega_\theta)\,\dot{\theta} + \left(\ddot{\theta}_{u\,\mathrm{lim}}\big/\omega_\theta^2\right) \\ \theta_{l\,\mathrm{lim}} &= \theta + (2\zeta_\theta/\omega_\theta)\,\dot{\theta} + \left(\ddot{\theta}_{l\,\mathrm{lim}}\big/\omega_\theta^2\right)\end{aligned} \qquad (28)$$

A saturation function can be used for limit avoidance in the command filter with upper and lower limits computed from Eq. (28). Because these constraints are implemented on the input to the command filter, they only affect the feedforward portion of the controller, effectively filtering pilot commands so that hub moment limits are not exceeded. Stability problems associated with saturations in the feedback loop are completely circumvented, greatly enhancing the robustness of this method. On the other hand, the method may not be as effective in avoiding hub moment limit violations that might occur due to feedback, for example, due to a strong gust disturbance.

IV. Results

The controller was evaluated using a nonlinear simulation model of the UH-60A Black Hawk (GENHEL).[20] The controller is applicable to fly-by-wire aircraft, thus the existing stability augmentation systems of the UH-60 were turned off and a fly-by-wire controller was simulated. Even though the existing Black Hawk helicopters are not fly by wire, the UH-60 and other U.S. Army rotorcraft are expected to be upgraded with fly-by-wire flight control systems in the near future. The system evaluated here is not limited to application on the UH-60. The GENHEL simulation model of the UH-60 was selected for evaluation because it is a level 2 simulation model[21] suitable for evaluating aircraft performance up to the operational flight envelope. This aspect is important when evaluating the limit protection system.

A. Controller Evaluation

The first task is to evaluate the tracking ability of the controller. A series of step commands is an appropriate maneuver for this purpose. Large magnitude inputs were used to evaluate the performance of the controller in the presence of significant nonlinear effects and large variations in flight conditions. Large magnitude inputs were also appropriate for evaluating the hub moment limiting system because they would be representative of the worst-case loads typically used in structural design. The objective of this section is to evaluate the tracking performance of the controller, and so the maneuvers were performed without the hub moment limiting system engaged. Evaluation for the hub moment limiting system is presented in a following section.

To evaluate the effect of adaptation on the controller response, the maneuvers were performed in two steps. During the first cycle of the maneuver, all of the ANN weights were forced to remain at zero value, thereby removing the effect of the neural network on the controller. This is also useful in evaluating the tracking ability of the model inversion controller without adaptation. After the first cycle, the adaptation was turned on, and the improvement due to adaptation was observed. The controller evaluation results are presented in Figs. 3–13.

Figure 3 shows an evaluation of roll angle command tracking at hover and low speed. A series of ±40-deg step commands in roll angle was given at hover and a forward speed of 30 kn. During the first cycle of the maneuver when the adaptation was off, the actual roll angle response was different from the commanded input. After the adaptation was turned on at 12 s, the roll angle response closely followed the commanded input. Moreover, as time progressed, the response became more accurate. This can be attributed to increase in the accuracy of the neural network as the sample data for training increases with advancing time.

The controller was designed to perform a coordinated turn for roll angle commands at high speed. This feature was evaluated by performing a 180-deg turning maneuver. The maneuver started with a trim speed of 80 kn and a step roll angle command of 25 deg was given for approximately 27 s. The aircraft performed a steady turn at approximately 6 deg/s. Aircraft response for this maneuver is shown

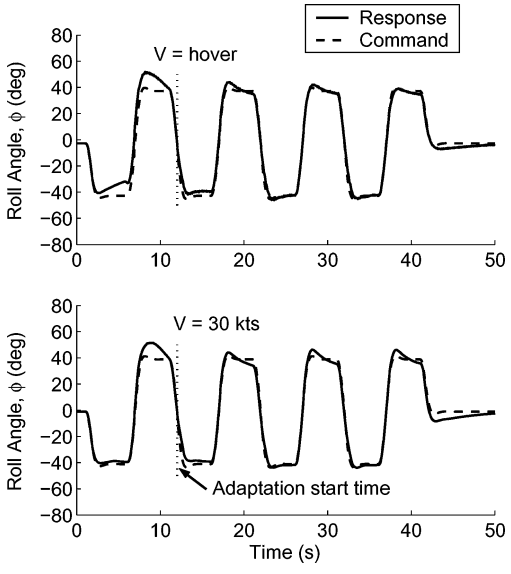

Fig. 3 Roll angle command tracking at low velocities.

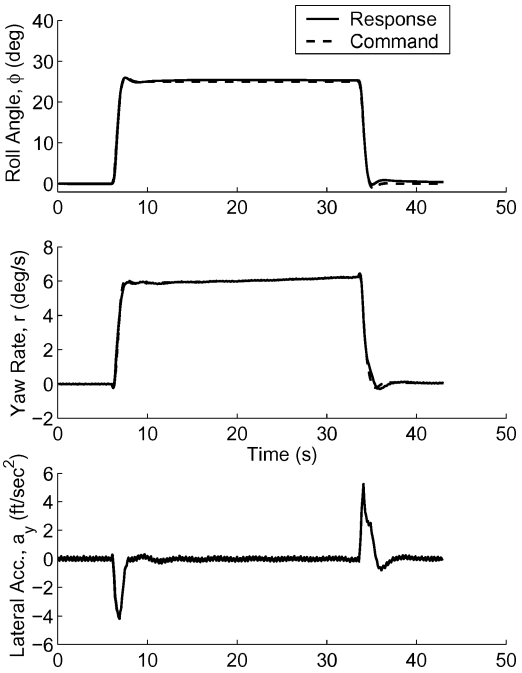

Fig. 4 Coordinated turn at high velocity.

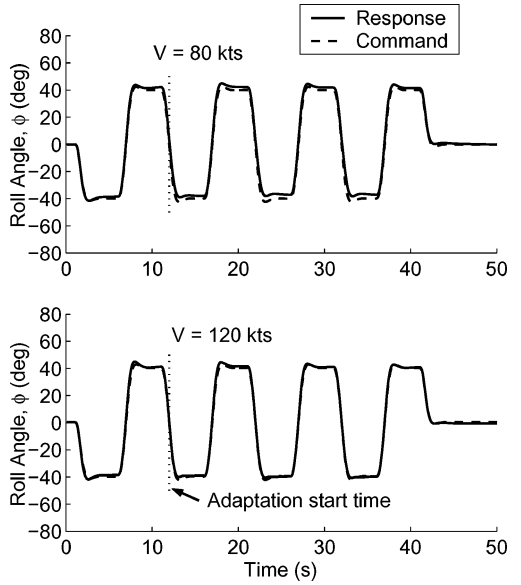

Fig. 5 Roll angle command tracking with coordinated turn at high velocities.

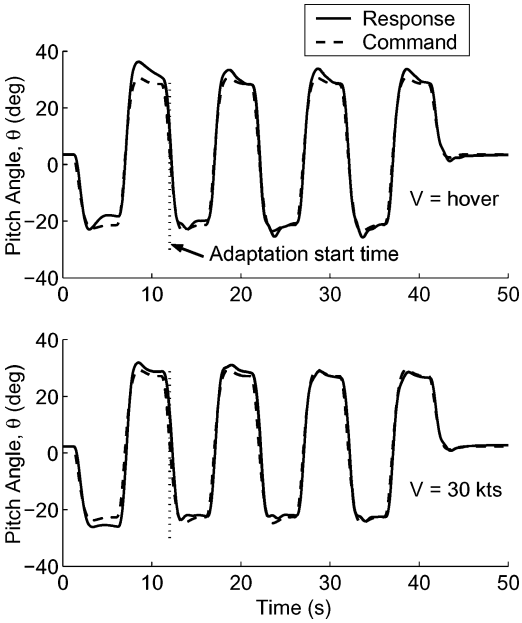

Fig. 6 Pitch angle command tracking at low velocities.

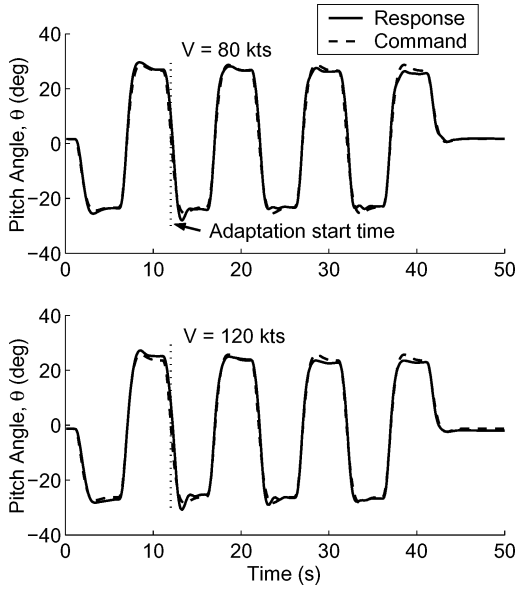

Fig. 7 Pitch angle command tracking at high velocities.

in Fig. 4. The yaw rate command was calculated using Eq. (17) to keep the lateral acceleration close to zero. The lateral acceleration is held constant at zero except during the transients associated with step command input.

Roll angle command tracking at high velocities is evaluated in Fig. 5. A ±40-deg step roll angle command was given at speeds of 80 and 120 kn. Because the linear model used for the model inversion controller was linearized at 80 kn, better tracking performance was obtained for these airspeeds as expected. In fact, the tracking was sufficiently good with the basic linear model that there was only minor improvement when the adaptation was turned on. Surprisingly, the command tracking was better in the 120-kn case than in the 80-kn case, even though the inversion model was based on a model linearized at 80 kn. This can be explained by the fact that the airspeed decreases through the course of the maneuver, and in the maneuver that started at 120 kn the airspeed approached closer to the design point of 80 kn over time.

Pitch angle command tracking evaluation for low and high velocities is shown in Figs. 6 and 7, respectively. At low velocities, a series of ±25-deg step commands in pitch angle was given. Figure 6 shows that the adaptation is shown to improve the tracking performance at low speed where the pitch dynamics are significantly different than the dynamics at the design point of 80 kn. Figure 7 shows that good tracking performance was obtained even without adaptation for both the design point (80 kn) and the off-design point (120 kn). The pitch dynamics at 120 kn are not substantially different from those at 80 kn.

Figure 8 shows the yaw rate command tracking at low velocities. The ANN was not used for the yaw channel because good tracking performance was obtained with the inversion model over a wide range of flight conditions. At high velocities, a lateral acceleration command was specified. The desired yaw rate command was computed from Eq. (17). The tracking performance for these velocities is shown in Fig. 9. Figures 9 show desirable tracking performance for all velocities.

Sample weight variation for the ANN is shown in Fig. 10. These weights were obtained for the response to a pitch angle command at hover shown in Fig. 6. The magnitude of the weights is irrelevant as the basis vectors were not normalized, but their variation with time

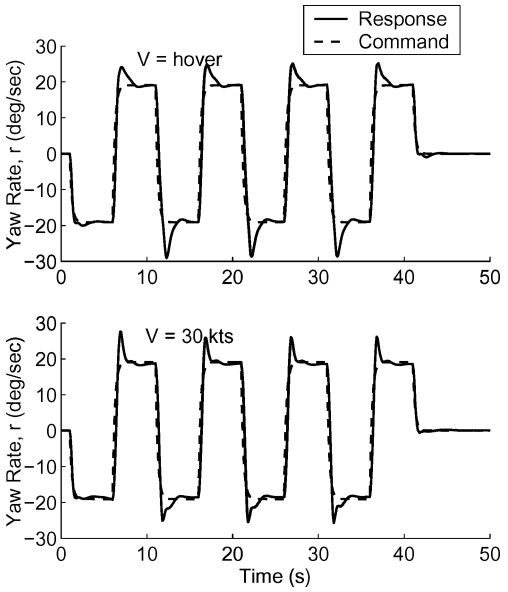

Fig. 8 Yaw rate command tracking at low velocities.

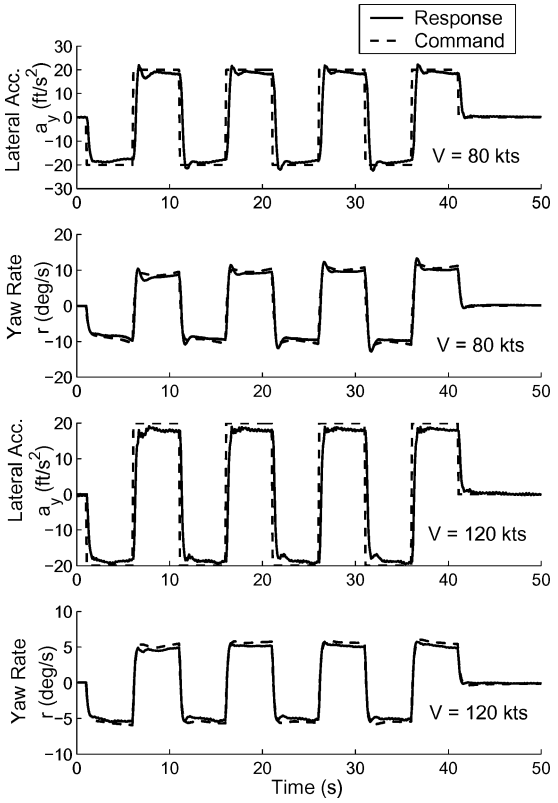

Fig. 9 Lateral acceleration command tracking at high velocities.

is more significant in evaluating the stability of the adaptation law. All of the weights were forced to remain at zero during the first cycle of the maneuver to evaluate the effect of the ANN on the controller response. The adaptation was turned on at 12 s. The initial weight value of zero is incorrect for the flight condition, and the weights update according to the adaptation law. The weights reach a steady value after each control input. Figure 10 also shows the forward velocity, sideslip, and descent velocities. Velocities are changing after each control input, and the weights are continuously adapting to the changing flight condition. The forward velocity is steadily varying for each control input corresponding to a quasi-steady variable, whereas the sideslip and descent velocity are continuously changing throughout the maneuver. A similar trend can be observed

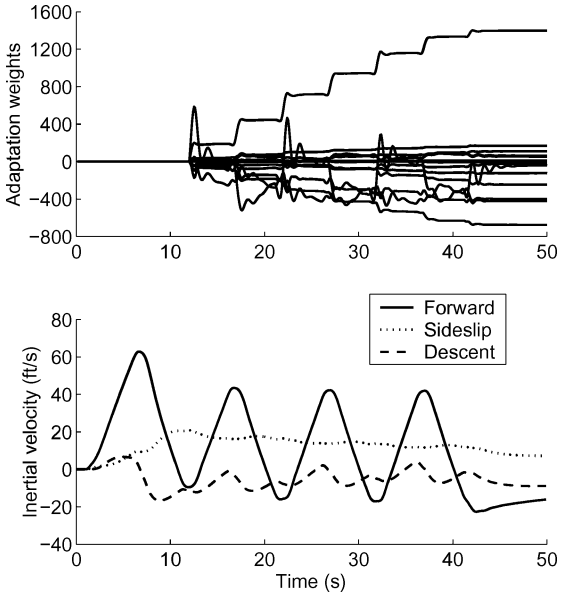

Fig. 10 Sample ANN weights for pitch command.

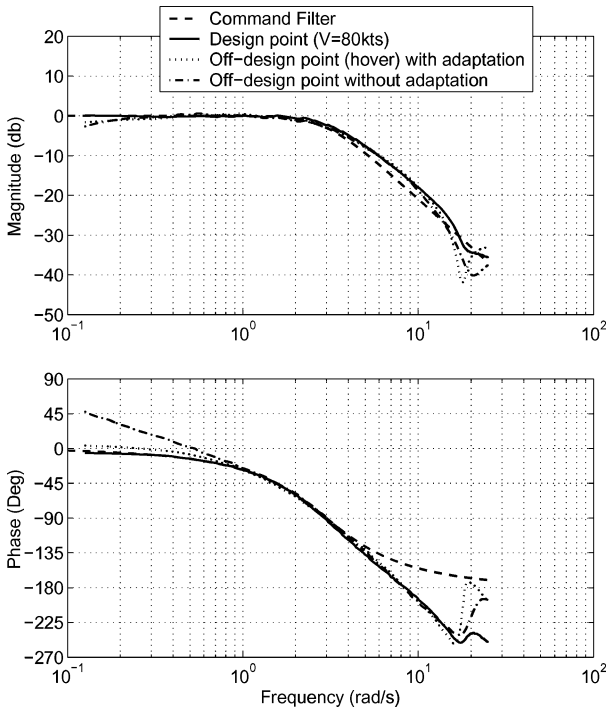

Fig. 11 Roll angle frequency response comparison.

in the weight variation where some weights reach a steady state immediately after a control input, whereas some weights are continuously adapting to the changing flight condition. At the end of the maneuver, all weights reached a steady value.

B. Frequency Response Evaluation

Figures 11–13 compare the closed-loop frequency response of the aircraft with the corresponding command filter response. The aircraft response was evaluated for three different flying conditions: 1) controller design point of 80 kn forward velocity, 2) off-design point evaluation at hover with and adaptation, and 3) off-design point evaluation at hover without adaptation. Before the evaluation input, the aircraft was perturbed using random inputs to allow the ANN weights to reach a steady state. To generate the frequency response, a chirp input was applied on the evaluation axis. The output was processed using CIFER to obtain the bode diagrams for the input/output

relationship.[22] These frequency response data were used to verify the compliance of the closed-loop aircraft with ADS-33 criteria (Table 1). The ADS-33 bandwidth in Table 1 corresponds to a −135-deg phase angle.[1]

Figure 11 shows the roll angle frequency response to a roll angle command input. The ADS-33 bandwidth obtained from the command filter was 5.5 rad/s. The bandwidth obtained from the frequency response at controller design point was 4.6 rad/s, which met the level 1 requirement of 2.5 rad/s for the highly maneuverable task of target acquisition and tracking. A reduction in the actual response bandwidth compared to the command filter bandwidth occurred because of the inherent aircraft time delays. Figure 12 shows the frequency response comparison for the pitch angle response. The actual response bandwidth of 3 rad/s was above the desired bandwidth of 2 rad/s required to meet the level 1 requirements for the task of target acquisition and tracking. Figure 13 shows the yaw rate frequency comparison. The actual bandwidth of 4 rad/s met the yaw angle bandwidth requirement (corresponding to the −45-deg frequency for yaw rate) of 3.5 rad/s.

Table 1 also lists the bandwidths for the off-design point hover flight. There was no significant difference in the bandwidth variation for this flight condition compared to the design point bandwidth. Also, Figs. 11 and 12 show greater improvement in phase angle with adaptation than without adaptation at hover. The adaptation effectively provided integral action to cancel the low-frequency errors.

C. Longitudinal Hub Moment Limit Evaluation

The longitudinal hub moment limiting system was evaluated using a series of step command inputs on the pitch angle. The hub moment limit was set to 20,000 ft · lb. This limit does not correspond to the structural limit of the Black Hawk. Conservative limiting was used here to evaluate the effectiveness of a structural load limiting system that might be used to reduce structural weight on an aircraft. The aircraft response to the pitch maneuver performed at 30 kn is shown in Fig. 14. Without the limiting system engaged, longitudinal hub moment significantly exceeded the limit. With the limiting system engaged, the peak response of the longitudinal hub moment stayed very close to the limiting value of 20,000 ft · lb. Figure 14 also shows the resulting change in the pitch angle response. The results show that only minor changes in the desired response resulted in significant reduction in the hub moment load. The pitch response was only slightly slower when the limiting system was engaged, but the magnitude of the peak hub moment was reduced from about 35,000 ft · lb to the limit value of 20,000 ft · lb. The longitudinal hub moment limiting effectively imposes a rate limit on the pitch angle command. The rate limit would vary depending on the magnitude of the pitch axis input. A similar maneuver performed at high velocities is shown in Fig. 15. For this maneuver the longitudinal hub moment also stayed very close to the limiting value of 20,000 ft · lb with relatively minor changes in the attitude rates.

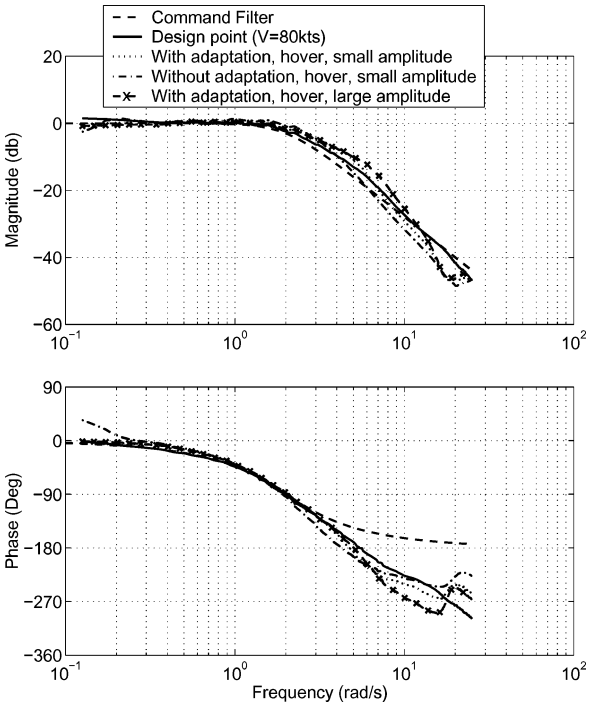

Fig. 12 Pitch angle frequency response comparison.

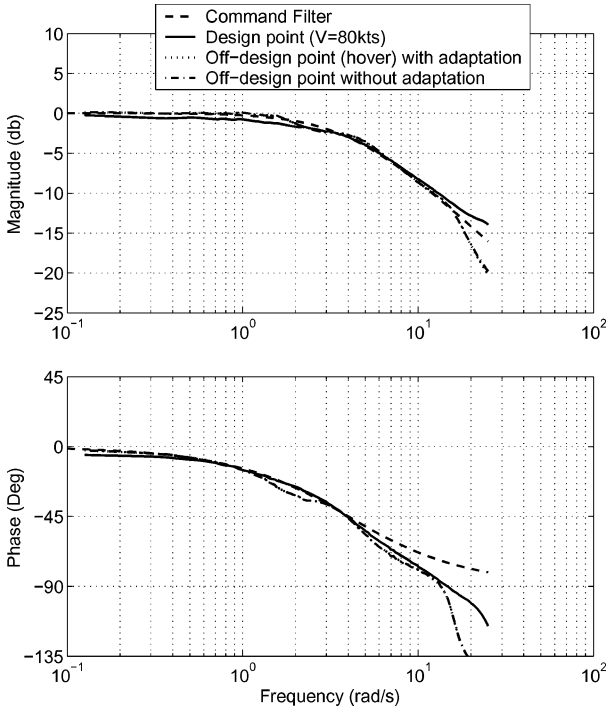

Fig. 13 Yaw rate frequency response comparison.

Table 1 Compliance with ADS-33 bandwidth requirements

		$V = 80$ kn		$V =$ hover adaptation		Handling qualities
Axis	Command filter	Ideal, rad/s	Actual, rad/s	On, rad/s	Off, rad/s	criterion[a]
Roll	Second order, $\omega_n = 3$ rad/s, $\zeta = 0.707$	5.5	4.6	5	4.9	Level 1
Pitch	Second order, $\omega_n = 2$ rad/s, $\zeta = 0.707$	3.5	3.3	3.3	2.8	Level 1
Yaw	First order, $\tau = 0.25$ s	4	4	4	4	Level 1

[a]Small-amplitude, low-velocity task of target acquisition and tracking.

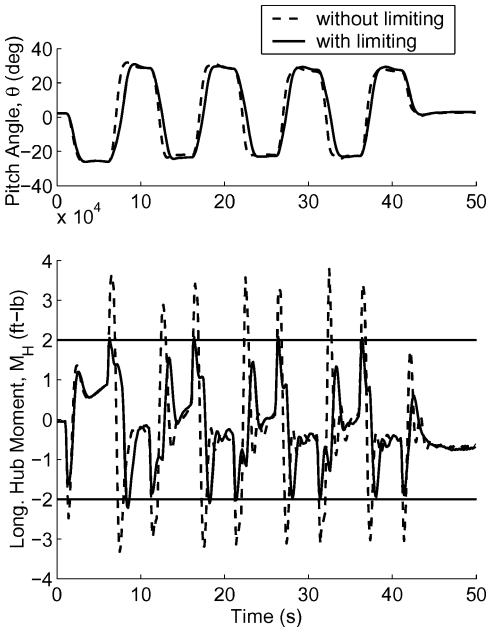

Fig. 14 Longitudinal hub moment limit avoidance at low velocity ($V = 30$ kn).

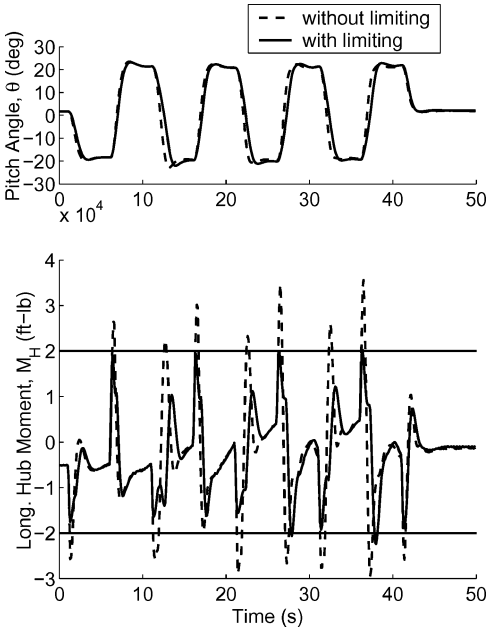

Fig. 15 Longitudinal hub moment limit avoidance at high velocity ($V = 80$ kn).

V. Conclusions

A high bandwidth adaptive model inversion controller has been evaluated in the present work to achieve ADS-33D handling qualities requirements in helicopters. A hub moment limit protection system was implemented by taking advantage of the ability of the controller to track attitude commands accurately. Specific conclusions drawn from this study include the following:

1) A model inversion controller was designed using a linear model at a single design point (80 kn). As expected, it was found that the controller had poor tracking performance in roll and pitch at some off-design points (particularly hover/low speed). The ANN improved the tracking performance without having to identify multiple linear models.

2) In some flight conditions, it was found that the basic model inversion controller performed quite well in the pitch and roll axes without adaptation.

3) It was found that selecting the error dynamics for the inversion controller to be of the same order as that of the command filter makes the overall system less prone to coupling with high-frequency rotor modes.

4) Consistent tracking performance was obtained for yaw rate command at all velocities without using an ANN. For the aircraft model used in this study, the added complexity of an ANN would not produce a significant performance increase in the yaw axis.

5) Neural network weights were continuously adapting to the changing flight condition. The weights quickly reach a steady state for a given flight condition.

6) The controller incorporated a coordinated turn feature at high velocities by computing the yaw rate command to keep the lateral acceleration zero. This proved to be an effective approach without requiring a complete reconfiguration of the yaw axis controller between low- and high-speed flight.

7) The closed-loop frequency response of the aircraft met the level 1 handling qualities requirements for the task of target acquisition and tracking. The actual aircraft bandwidth was smaller than the ideal command filter bandwidth because of the inherent time delays. This factor was accounted for in selection of the command filter response by selecting the command filter bandwidth to be little higher than the required specifications.

8) A longitudinal hub moment limiting system was implemented by constraining the pitch angle command in the command filter. The approach does not affect the feedback path of the controller, and, therefore, the stability of the closed-loop system is not affected by the load limiting.

9) Evaluation for the longitudinal hub moment limit avoidance was performed at low and high velocities. The transient peak of the longitudinal hub moment approached, but did not significantly exceed, the limiting value. The hub moment limiting resulted in minor changes in the pitch response of the aircraft for large magnitude inputs. The system was effective in avoiding the longitudinal hub moment limit without imposing conservative restrictions on the aircraft agility.

10) An airspeed scheduled model inversion controller might prove to be equally effective for this application (as opposed to an adaptive approach). Note that the hub moment limiting method presented here could also be applied to a scheduled controller as long as the controller accurately tracks pilot commands.

Acknowledgments

This research is funded by the National Rotorcraft Technology Center, under the Pennsylvania State University Rotorcraft Center Grant.

References

[1]"Aeronautical Design Standard Performance Specification: Handling Requirements for Military Rotorcraft," U.S. Army Aviation and Troop Command, Rept. ADS-33D-PRF, Redstone Arsenal, AL, May 1996.

[2]Kothmann, B. D., and Armbrust, J., "RAH-66 Comanche Core AFCS Control Law Development: DEMVAL to EMD," *Proceedings of the American Helicopter Society 58th Annual Forum*, American Helicopter Society, Alexandria, VA, 2002, pp. 523–546.

[3]Whalley, M. S., Hindson, W. S., and Thiers, G. G., "A Comparison of Active Sidestick and Conventional Inceptors for Helicopter Flight Envelope Tactile Cueing," *Proceedings of the American Helicopter Society 56th Annual Forum*, Vol. 1, American Helicopter Society, Alexandria, VA, 2000, pp. 181–204.

[4]Menon, P. K., Iragavarapu, V. R., and Whalley, M. S., "Estimation of Rotorcraft Limit Envelopes Using Neural Networks," *Proceedings of the American Helicopter Society 52nd Annual Forum*, American Helicopter Society, Alexandria, VA, 1996, pp. 1423–1431.

[5]Slotine, J. E., and Li, W., *Applied Nonlinear Control*, Prentice–Hall, NJ, 1991.

[6]Menon, P. K. A., Badgett, M. E., Walker, R. A., and Duke, E. L., "Nonlinear Flight Test Trajectory Controllers for Aircraft," *Journal of Guidance, Control, and Dynamics*, Vol. 10, No. 1, 1987, pp. 67–72.

[7]Snell, S. A., Enns, D. F., and Garrard, W. L., "Nonlinear Inversion Flight Control for a Supermaneuverable Aircraft," *Journal of Guidance, Control, and Dynamics*, Vol. 15, No. 4, 1992, pp. 976–984.

[8]Brinker, J. S., and Wise, K. A., "Stability and Flying Qualities Robustness of a Dynamic Inversion Robust Control Law," *Journal of Guidance, Control, and Dynamics*, Vol. 19, No. 6, 1996, pp. 1270–1277.

[9]Kim, B. S., and Calise, A. J., "Nonlinear Flight Control Using Neural Networks," *Proceedings of the AIAA Guidance, Navigation and Control Conference*, AIAA, Washington, DC, 1994, pp. 930–940.

[10]Leitner, J., Calise, A., and Prasad, J. V. R., "Analysis of Adaptive Neural Network for Helicopter Flight Control," *Proceeding of the AIAA Guidance, Navigation and Control Conference*, AIAA, Washington, DC, 1995, pp. 871–879.

[11]Rysdyk, R. T., and Calise, A. J., "Adaptive Model Inversion Flight Control for Tiltrotor Aircraft," *Proceedings of the American Helicopter Society 54th Annual Forum*, American Helicopter Society, Alexandria, VA, 1998, pp. 1356–1367.

[12]Johnson, E. N., and Kannan, S. K., "Adaptive Flight Control for an Autonomous Unmanned Helicopter," AIAA Paper 2002-4439, 2002.

[13]Horn, J. F., Calise, A. J., and Prasad, J. V. R., "Flight Envelope Cueing on a Tilt-Rotor Aircraft Using Neural Network Limit Prediction," *Journal of the American Helicopter Society*, Vol. 46, No. 1, 2001, pp. 23–31.

[14]Horn, J. F., Calise, A. J., and Prasad, J. V. R., "Flight Envelope Limit Detection and Avoidance for Rotorcraft," *Journal of the American Helicopter Society*, Vol. 47, No. 4, 2002, pp. 253–262.

[15]Yavrucuk, I., Prasad, J. V. R., and Calise, A. J., "Adaptive Limit Detection and Avoidance for Carefree Maneuvering," AIAA Paper 2001-4003, 2001.

[16]Yavrucuk, I., Unnikrishnan, S., and Prasad, J. V. R., "Envelope Protection in Autonomous Unmanned Aerial Vehicles," *Proceedings of the American Helicopter Society 59th Annual Forum*, American Helicopter Society, Alexandria, VA, 2003, pp. 2000–2010.

[17]Einthoven, P. G., Miller, D. G., Nicholas, J. S., and Margetich, S. J., "Tactile Cueing Experiments with a Three Axis Sidestick," *Proceedings of the American Helicopter Society 57th Annual Forum*, Vol. 1, American Helicopter Society, Alexandria, VA, 2001, pp. 779–794.

[18]Horn, J. F., and Sahani, N., "Detection and Avoidance of Main Rotor Hub Moment Limits on Rotorcraft," *Journal of Aircraft*, Vol. 41, No. 2, 2004, pp. 372–379.

[19]Sahani, N. A., Jeram, G. J., Horn, J. F., and Prasad, J. V. R., "Hub Moment Limit Protection Using Neural Network Prediction," *Proceedings of the American Helicopter Society 60th Annual Forum*, American Helicopter Society, Alexandria, VA, 2004, pp. 775–786.

[20]Howlett, J. J., "UH-60A BLACK HAWK Engineering Simulation Program: Volume I—Mathematical Model," NASA CR-177542, 1989; also U.S. Army Aviation Systems Command, TR 89-A-001, NASA Ames Research Center, Moffet Field, CA, Sept. 1989.

[21]Padfield, G. D., *Helicopter Flight Dynamics: The Theory and Application of Flying Qualities and Simulation Modeling*, AIAA, Education Series, AIAA, Washington, DC, 1995.

[22]Tischler, M. B., and Cauffman, M. G., "Frequency Response Methods for Rotorcraft System Identification: Flight Application to BO-105 Coupled Rotor/Fuselage Dynamics," *Journal of American Helicopter Society*, Vol. 37, No. 3, 1992, pp. 3–17.